High Performance Yacht Design Conference
Auckland, 4-6 December, 2002

RANSE SIMULATIONS FOR SAILING YACHTS INCLUDING DYNAMIC SINKAGE & TRIM AND UNSTEADY MOTIONS IN WAVES

Rodrigo Azcueta[1], rodrigo@azcueta.net

Abstract: This paper presents RANSE computations of steady flows around sailing yachts including the dynamic sinkage and trim, and simulations of unsteady boat motions in incident waves. The steady flow computations efficiently yield the complete resistance curve in one go – from zero to maximum boat speed – instead of computing only for one boat speed at the time. This allows to compare differences in resistance for the entire F_n-range e.g. due to small modifications in the boat's shape or due to shifting the centre of mass of the boat. The simulations of boat motions in waves aim to show that the method is robust enough and well suited for simulating the boat's responses to waves coming from any direction. With CPU times of a few hours on common personal computers for each characteristic wave, this method promises great potential for the near future.

NOMENCLATURE

B	Reference beam
β	Yaw or leeway angle
DOF	Degrees-Of-Freedom
F_n	Froude number
φ	Roll or heel angle
G	Centre of mass
H_w	Wave height
L	Reference length
λ_w	Wave length
LCG	Longitudinal Centre of Gravity
μ_w	Wave direction relative to boat course
RANSE	Reynolds Averaged Navier-Stokes Equations
R_n	Reynolds number
RS	Reference System
T_e	Period of wave encounter
θ	Pitch or trim angle
v_o	Mean boat speed
ω_e	Frequency of wave encounter
ζ_w	Wave amplitude

1. INTRODUCTION

RANSE computations are rapidly spreading in high-performance yacht design offices, especially those working for big budget campaigns, such as the America's Cup or the Volvo Ocean Race. A popular approach to CFD-based performance prediction for sailing yachts has long consisted in computing the wave-making resistance with panel codes based on potential theory and in optimising appendages by means of RANSE solvers. In recent years, however, a real breakthrough in RANSE computations was accomplished with the implementation and validation of free-surface flows. Since then free-surface RANSE computations are increasingly becoming a central tool for practical yacht design.

For sailing yachts (and also any vessel sailing at a high F_n, like power boats) the change in the boat's running attitude (sinkage, trim, heel) due to the pressure field around the hull is quite significant so that its effects influence performance to a large extent and should be taken into account. But to date this has usually been neglected in RANSE computations, which instead compute the flow around the boat fixed in a given position, either in the floating attitude at rest or in the running attitude measured in the towing tank. A few exceptions are rudimentary approaches to take sinkage and trim into account in an iterative manner without really coupling the fluid flow and body motions.

In this work, a more general approach was implemented, extending a Navier-Stokes code to couple the fluid flow with the body motions induced by the flow and/or by external forces. This allows not only to compute dynamic sinkage and trim but also to simulate the unsteady boat motions in the 6 DOF. The fundamentals of this approach were implemented and validated as a doctoral thesis [1]. Here, only the application to sailing yachts will be demonstrated.

2. NUMERICAL METHOD

To couple the fluid flow and body motions I extended the Navier-Stokes solver COMET with a *body-motion module*. COMET is a commercial code developed in Germany by ICCM GmbH, now a member of the CD Adapco Group, the developers of the well-known multi-purpose STAR-CD code. COMET was one of the first Navier-Stokes codes to implement a modern free-surface feature specially tailored to suit the needs of the naval industry. It is therefore best suited for computing problems related to naval hydrodynamics such as free-surface flows including wave-breaking, sprays and cavitation, as well as turbulent flows with well proven turbulence models.

The general idea for coupling the fluid flow with the body motions is as follows: the Navier-Stokes flow solver computes the flow around the body in the usual way, taking into account the fluid viscosity, flow turbulence and deformation of the free surface. The forces and moments acting on the body are then calculated by integrating the normal

[1]Independent CFD consultant, www.azcueta.net
Project manager ship design, MTG Marinetechnik, Hamburg

(pressure) and tangential (friction) stresses over the body surface. Following this, the body-motion module solves the equations of motion of the rigid body in the 6 DOF using the forces and moments calculated by the flow solver as input data. The motion accelerations, velocities and displacements (translations and rotations) are obtained by integrating in time. The position of the body is updated and the fluid flow is computed again for the new position. By iterating this procedure over the time, the body trajectory is obtained.

Calculations with this method including the dynamic sinkage and trim (steady-state case) were validated for the Series 60 hull (a well-known benchmark model widely used for validation of hydrodynamic computations) and for the model of a very fat ship with a blunt bow similar to a tanker (which is used as a benchmark for breaking-wave computations). These two examples showed that the method works well for very tiny changes in sinkage, trim (and also heel for the drift sailing condition) as well as for very large ones. The inclusion of the dynamic sinkage and trim in the calculations improved the agreement with experiments, and thus performance prediction.

Simulations of unsteady body motions were validated for 2-D drop tests with a wedge (used for slamming investigations). Comparisons with experiments proved very good agreement for both magnitude and timing of the accelerations, velocities and motions [1]. A validation for a 3-D case was also carried out for the model of a naval combatant in head waves and 2 DOF (heave and pitch) and showed good agreement with experiments. Slamming and green water on deck were simulated as well. In all these simulations the body trajectory, velocity and accelerations are obtained from the flow forces and/or external forces acting on the body without the need for prescribing the body trajectory.

2.1 Body-motion module

Two orthogonal Cartesian reference systems (RS) are used: A non-rotating, non-accelerating Newtonian RS (O, X, Y, Z) which moves forward with the mean ship speed, and a body-fixed RS (G, x, y, z) with origin at G, the centre of mass of the body. The undisturbed free-surface plane always remains parallel to the XY plane of the Newtonian RS. The Z-axis points upwards. The x-axis of the body-fixed RS is directed in the main flow direction, i.e. from bow to stern, the y-axis is taken positive to starboard and the z-axis is positive upwards. The body motions are executed using a *single-grid strategy*, where a rigid, body-fixed grid moves relative to the Newtonian RS, and the ficticious flow forces due to the grid movement are automatically taken into account in the flow equations. The body-motion module is linked and run simultaneously with the flow solver and can operate and update all flow variables, boundary conditions and parameters of the numerical method.

The motion of the rigid body in the 6 DOF are determined by integrating the equations of variation of linear and angular momentum written in the form referred to G (all vector components expressed in the Newtonian RS):

$$m\ddot{\vec{X}}_G = \vec{F} \tag{1}$$

$$\overline{\overline{T}}\,\overline{\overline{I}}_G\overline{\overline{T}}^{-1}\dot{\vec{\Omega}} + \vec{\Omega} \times \overline{\overline{T}}\,\overline{\overline{I}}_G\overline{\overline{T}}^{-1}\vec{\Omega} = \vec{M}_G \tag{2}$$

where m is the body mass, $\ddot{\vec{X}}_G$ the absolute linear acceleration of G, $\vec{F}$ is the total force acting on the body, $\dot{\vec{\Omega}}$ and $\vec{\Omega}$ are the absolute angular acceleration and angular velocity, respectively, and $\vec{M}_G$ is the total moment with respect to G, $\overline{\overline{I}}_G$ is the tensor of inertia of the body about the axes of the body-fixed RS, $\overline{\overline{T}}$ is the transformation matrix from the body-fixed into the Newtonian RS.

The contributions to the total force and to the total moment acting on G are:

$$\vec{F} = \vec{F}_{flow} + \vec{W} + \vec{F}_{ext} \tag{3}$$

$$\vec{M}_G = \vec{M}_{G_{flow}} + (\vec{X}_{ext} - \vec{X}_G) \times \vec{F}_{ext} \tag{4}$$

where $\vec{F}_{flow}$ and $\vec{M}_{G_{flow}}$ are the total fluid flow force and moment determined by integrating the normal (pressure) and tangential (friction) stresses, obtained from the Navier-Stokes solver. They include the static and the dynamic components of the water and of the air flow. $\vec{W}$ is the body weight force. $\vec{F}_{ext}$ can be any external force acting on the body which one wants to introduce to simulate for instance the sail forces and moments.

The boat motions are described in each time instant by the position of its centre of gravity $\vec{X}_G$ and the body orientation given by $\overline{\overline{T}}$. Surge, sway and heave are defined in this work as the translations of G in the directions of the Newtonian RS. The angles of rotation are defined in the following order: First the rotation around the vertical axis in the Newtonian RS (yaw or leeway angle), second the rotation around the new transverse axis (pitch or trim angle), and last the rotation around the new longitudinal axis (roll or heel angle). To integrate in time the equations of motion a first-order explicit discretisation method has shown to work well and is used preferably. Instead of integrating the angular velocity $\vec{\Omega}$ to obtain the rotation angles, the new orientation of the body is found by integrating the unit vectors of the body-fixed RS, which are the columns of $\overline{\overline{T}}$. For details on the body-motion module see [1].

2.2 Flow solver

The solution method in COMET is of finite-volume-type and uses control volumes with an arbitrary number of faces (unstructured meshes). It allows cell-wise local mesh refinement, non-matching grid blocks, and moving grids with sliding interfaces. The integration in space is of second order, based on midpoint rule integration and

linear interpolation. The method is fully implicit and uses quadratic interpolation in time through three time levels.

The deformation of the free surface is computed with an *interface-capturing scheme* of VOF type (Volume Of Fluid), which has proven to be well suited for flows involving breaking waves, sprays, hull shapes with flat stern overhangs and section flare, etc, see [2]. In this method, the solution domain covers both the water and air region around the hull and both fluids are considered as one effective fluid with variable properties. An additional transport equation for a void fraction of liquid is solved to determine the interface between the two fluids. The *High-Resolution-Interface-Capturing* (HRIC) discretisation scheme for convective fluxes in the void fraction equation is used to ensure the sharpness of the interface.

The solution method is of pressure-correction type and solves sequentially the linearised momentum equations, the continuity equation, the conservation equation of the void fraction, and the equations for the turbulence quantities. The linear equation systems are solved by conjugate gradient type solvers and the non-linearity of equations is accounted for by Picard iterations. The method is parallelised by domain decomposition in both space and time and is thus well suited for 3-D flow computation with free surfaces – especially when they are unsteady, as in the case of freely-floating bodies – since they require a lot of memory and computing time. For details on the flow solver see [3].

2.3 Numerical mesh and simulation set-up

All examples presented here were carried out for a Yacht of type Judel/Vrolijk Dehler 33 ($L = 10$ m). This boat has been extensively used to investigate sailing forces under real conditions by means of a full-scale sailing dynamometer at the Technical University of Berlin, [4]. The same numerical mesh was used for both the steady flow calculations and the unsteady boat motions. It was generated using the ICEM-CFD Hexa mesh generator. Although it is relatively coarse with about $100{,}000$ control volumes each side of the boat, the computed flow and boat motions are well captured and CPU times are kept low. Figure 1 shows the surface mesh for the hull, keel and rudder. The mesh was conceived to allow large rolling motions of up to $30\,^\circ$ without the top boundary dipping into the water. The computational domain extends for about $1\,L$ to the front, back, sides and bottom, cf. Figure 8.

The longitudinal position of G was calculated for the boat in the upright condition floating on an even keel. The vertical position of G was set at the height of the design waterline. The roll radius of gyration was set to $k_{x_G} = 0.33\,B$ and the pitch radius of gyration was set to $k_{y_G} = 0.15\,L$. The products of inertia were set equal to zero. The front, side, bottom and top flow-boundaries were specified as an inlet of constant known velocity (boat speed in opposite direction) and known void fraction distribution defining the water and air regions. The wake flow-boundary was specified as a zero-gradient boundary of known pressure distribution (hydrostatic pressure). All calculations were performed for the full-scale boat using the standard k-ϵ turbulence model with wall functions ($R_n < 8 \cdot 10^7$).

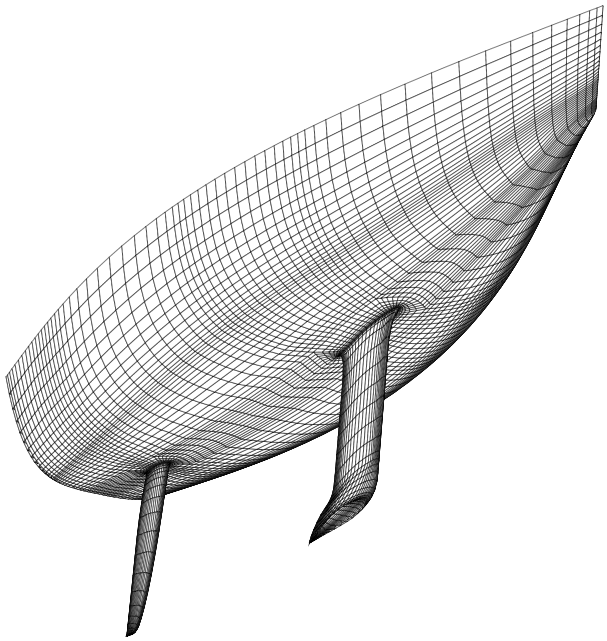

Figure 1. Surface mesh generated with ICEM-CFD Hexa

3. RESISTANCE TESTS

RANSE computations are usually carried out for a given boat speed at a time and then repeated for as many speeds as are of interest. Here, the entire resistance curve is obtained in one single run. To achieve this, the boat, starting from the position at rest, accelerates very slowly with a constant acceleration until it reaches the maximum boat speed expected. Since the acceleration is small and the flow basically converges for each instant boat speed, the calculation can be considered to be quasi-steady. The CPU time is obviously greater than when computing only one boat speed, but it pays off if many boat speeds are to be computed. The accuracy of the resistance prediction is the same as the one obtained when computing for each boat speed until convergence is reached (after about $4{,}000$ time steps). Note that although the flow is steady once converged, since the free surface has to develop its final wave pattern, the computations have to be carried out iterating in time, i.e. solving the transient terms of the flow equations.

3.1 Basis boat upright

Figure 2 shows a typical resistance test computed in this way for the boat in the upright position. The solid line represents the resistance curve. It was performed for a F_n-range from zero to 0.7. As has been mentioned earlier, the most important feature of these computations is that the dynamic sinkage and trim are computed throughout

the entire F_n-range. These curves are given in Figure 2 as well. Since the boat is free to sink and trim, the heave force is constant (in the diagram it balances the boat weight, $\vec{W} \approx 30{,}000$ N) and the pitch moment is constant and equal to zero. The computed results are in very good agreement with the extrapolation to full-scale from the experimental measurements with a 5 m model at the Ship Model Basin in Potsdam (SVA), for the measured F_n-range of 0.22 to 0.38.

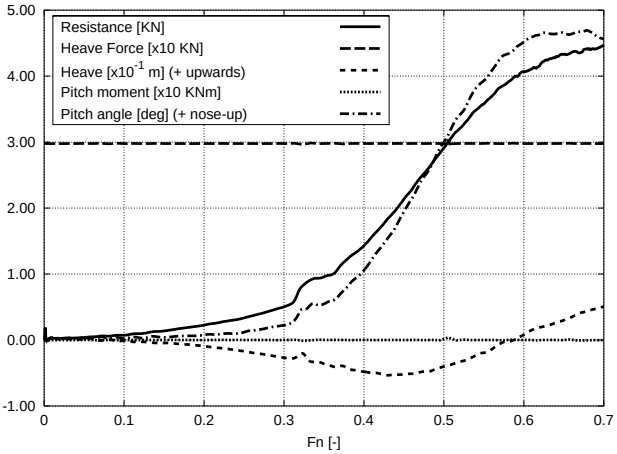

Figure 2. Resistance curve for the boat free to sink and trim

For purposes of comparison Figure 3 shows the resistance test for the case of the boat fixed in the floating position at rest (upright) throughout the entire F_n-range. In this diagram the heave and pitch curves are constant and equal to zero and the heave force and pitch moment contain the dynamic component due to the flow so that they vary with varying boat speed. Figure 4 and 5 show isobars and the wave contour at the highest computed boat speed (7 m/s) for the case of the boat free to sink and trim and the case of the boat in the fixed position, respectively. For the latter case, the computed solution at high F_n is obviously not realistic, and so is the computed resistance curve.

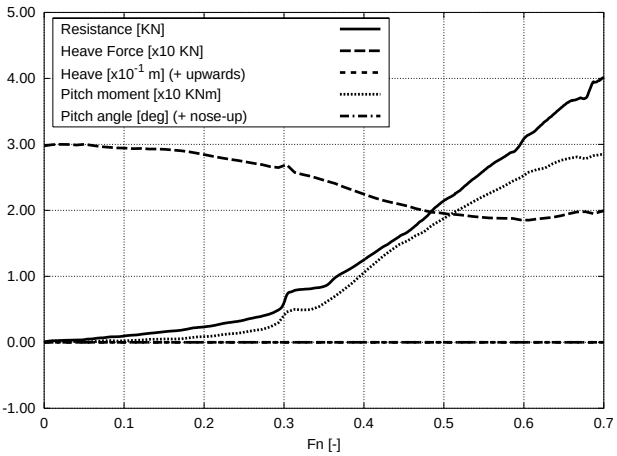

Figure 3. Resistance curve for the boat in a fixed position

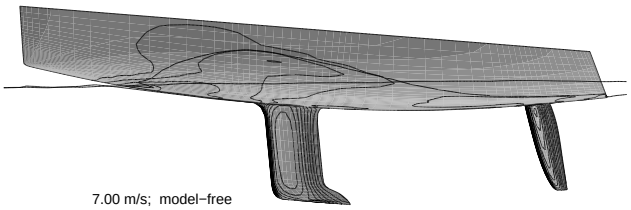

Figure 4. Isobars and wave profile for the boat free to sink and trim

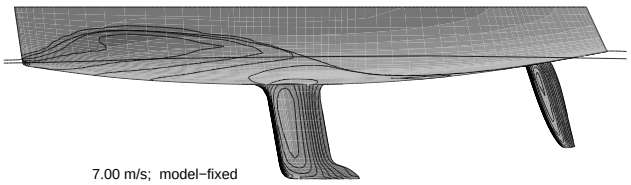

Figure 5. Isobars and wave profile for the boat in a fixed position

The CPU time needed for computing the numerical resistance test of Figure 2 was 8 hours on a linux-cluster with 4 AMD 2000+ processors, or something less than 4 times that on a single processor. A total of $35{,}000$ outer iterations were needed, with 5 outer iterations per time step, a time step size of 0.01 s and an acceleration of 0.1 m/s^2.

3.2 Basis boat upwind

Figure 6 shows the resistance test for the boat sailing in one upwind condition, i.e. with a heel angle $\varphi = -15^\circ$ (negative means heeled to Stb) and a leeway angle $\beta = 4^\circ$ (positive means flow from Stb). Without changing LCG the boat floats at rest with a trim angle $\theta = -1.5^\circ$ (negative means nose down). 3 DOF are free in this case: Heave, roll and pitch. The leeway angle is kept fixed, since the computation does not include any course controller yet. A constant external roll moment of about $M_{G_x} \approx -9000$ Nm was set to heel the boat -15° at rest and applied throughout the entire F_n-range. It is interesting to see how the roll

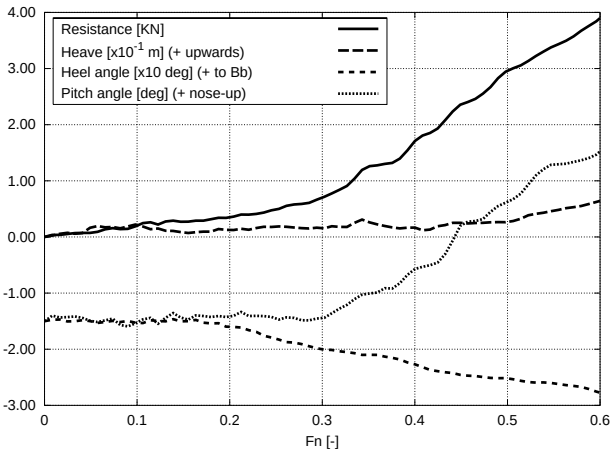

Figure 6. Resistance curve for the boat free to sink, trim and heel sailing upwind

angle increases with speed due to the increasing lift on the appendages.

3.3 Modified boats

To show how this way of computing the resistance curves can be applied to optimization, the boat's shape was slightly varied in three steps and the differences in resistance for the upright condition were calculated. A quick variation in boat shape was achieved by scaling the numerical mesh in longitudinal and transverse direction, while keeping the displacement unchanged. The different versions are named *Mod-1*, *Mod-2* and *Mod-3*. *Mod-1* e.g. is obtained by elongating the basis boat by 0.25% in x-direction (2.5 cm) and compressing it by 0.25% in y-direction. Table I summarises the three modifications. The resulting LCG is given measured from the bow.

Table I. Modifications of the basis boat

	Basis	Mod-1	Mod-2	Mod-3
x-direction [% of L]	-	$+0.25$	$+0.5$	$+1.0$
y-direction [% of B]	-	-0.25	-0.5	-1.0
LCG [m]	4.848	4.861	4.873	4.897

Figure 7 shows the differences in resistance (Δ resistance) compared to the basis boat for the three modifications averaged in steps of 0.1 of F_n for the entire F_n-range. The deltas are all negative meaning a reduction in resistance. From this diagram one can see for instance that for the F_n-range between 0.4 and 0.5 the *Mod-1* has 0.6%, *Mod-2* has 1.2% and *Mod-3* has 2.6% less resistance than the basis boat. The differences in resistance averaged over the entire F_n-range ($0.0 - 0.7$) are given in Table II. The way one would average the results depends on how this data is to be handled by the VPP used, i.e. if it uses discrete resistance values or if it can handle the raw data.

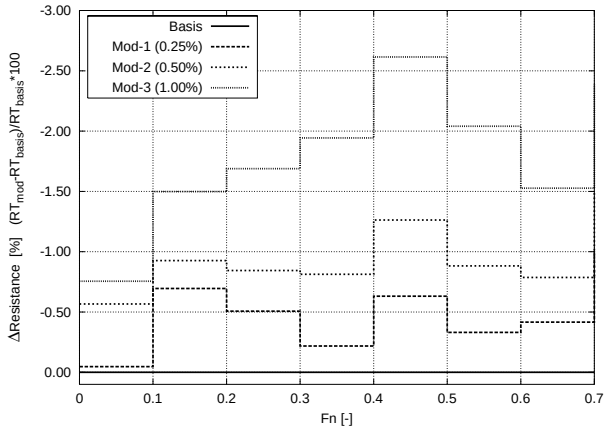

Figure 7. Δ resistance as a function of F_n

Table II. Δ resistance averaged over the entire F_n-range

	Basis	Mod-1	Mod-2	Mod-3
Δ Resistance	–	-0.4%	-0.9%	-1.8%

4. BOAT IN INCIDENT WAVES

Prior to the simulations with the boat in waves shown here, the motions of the boat floating freely at the free surface in calm water were simulated. These motions were induced by releasing the boat from a position where the hydrostatic forces were out of equilibrium or by exciting the boat through an external sinusoidal roll moment. Both types of tests – roll extinction and roll excitation tests – were used to quantify the viscous roll damping of the boat with appendages at different speeds, [1]. Following this, the boat responses to incident regular, long-crested waves were simulated. Only these examples are shown here.

The incident waves are generated at the inlet flow-boundary by imposing the instantaneous wave elevation and orbital velocities according to the linear wave theory. The orbital velocities of the waves are thus superimposed to the mean flow velocity. Three wave parameters are set at the beginning of a simulation: The wave amplitude ζ_w, the wave length λ_w and the wave direction μ_w relative to the boat course ($\mu_w = 0^\circ$ means from astern and $\mu_w = 90^\circ$ from port). Due to numerical diffusion the wave amplitude hitting the boat is reduced to some extent, although it is surprising that such a coarse mesh already produces relatively good results.

Figure 8 shows the boat in the upwind position in oblique waves. This example will be presented next. The figure shows the edges of the computational domain, whereby the top flow-boundary has a deadrise of 30° to allow for large roll angles. Also shown is the cut of the computational domain with the undisturbed waterplane. In the single-grid strategy used in these simulations, the computational domain moves as a whole relative to this plane. The boundary conditions – the mean flow velocity, the orbital velocity, the void fraction distribution defining the wave elevations, the turbulence parameters and so on – have to be very carefully imposed at each time instant relative to the undisturbed waterplane. The VOF method and the implemented boundary conditions have proven to be very robust, since the free surface can leave the computational domain in any place, i.e. through the top flow-boundary in case that the boat heels or pitches with a large angle. Even a capsize upside down would be possible.

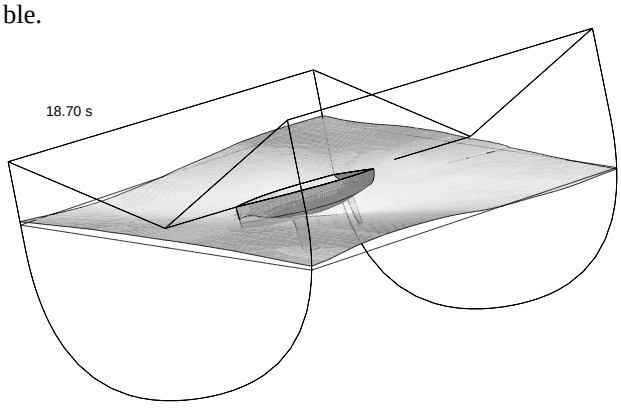

Figure 8. Boat beating to windward in waves

4.1 Boat upwind in waves

To set-up this simulation, the sailing forces for the boat sailing in an upwind condition ($\varphi = -15°$, $\beta = 4°$ and $v_o = 3.5$ m/s) were first calculated in calm water. Following this the simulation in waves was started and the previously calculated sail forces and moments were kept constant throughout the simulation (i.e. a driving force $F_x = -1045$ N and a heeling moment $M_{G_x} = -5631$ Nm). 4 DOF were set free: Surge, heave, roll and pitch. The wave parameters were chosen as follows: Wave amplitude $\zeta_w = 0.25$ m (wave height $H_w = 0.5$ m), wave length $\lambda_w = 20$ m and wave direction $\mu = 135°$. This results in a frequency of wave encounter $\omega_e = 2.5$ s^{-1} ($T_e = 2.5$ s). The waves thus come obliquely at an angle of $45°$ from the bow and hit the port side at intervals of 2.5 s.

Figure 9 shows the computed motions in the 4 DOF and also the variation in boat speed (v_{sea}) for the last 10 s simulation time. In the first few seconds simulation time the motions are still irregular, since the waves have to build up first. After 10 s simulation time the boat responses are periodical, with a period corresponding to T_e. The roll angle oscillates between about $-13°$ and $-18°$. The pitch angle oscillates between about $-6°$ and $+2.5°$. The heave, measured at G, oscillates between about -0.3 m and $+0.3$ m. Note that the wave amplitude was $\zeta_w = 0.25$ m.

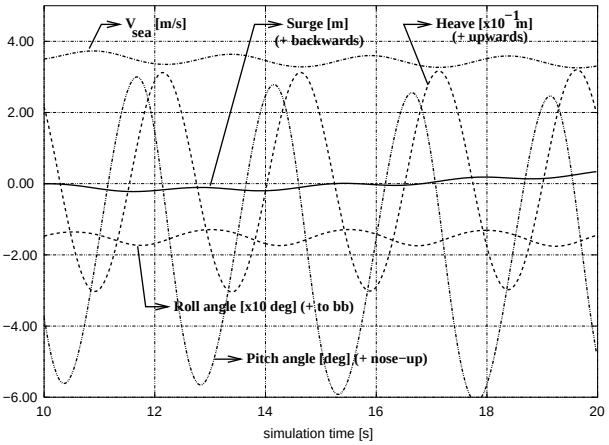

Figure 9. Motions of boat sailing upwind in waves

Figure 10 shows the computed forces and moments for the 6 DOF for the last 10 s simulation time. The mean heave force balances the boat weight, $\vec{W} \approx 30{,}000$ N. The mean resistance and mean roll moment balance the external driving force and heeling moment, respectively. Since the boat is constrained in sway and yaw, the variations in side force and yaw moment induced by the waves are relatively large, i.e. the side force amplitude is of the order of the heave force amplitude and the the yaw moment amplitude is of the order of the pitch moment amplitude. The forces and moments are $180°$ out of phase with the corresponding motions. Note that the forces and moments are usually more sensitive to high-frequency numerical oscillations than the integrated motion velocities and displacements.

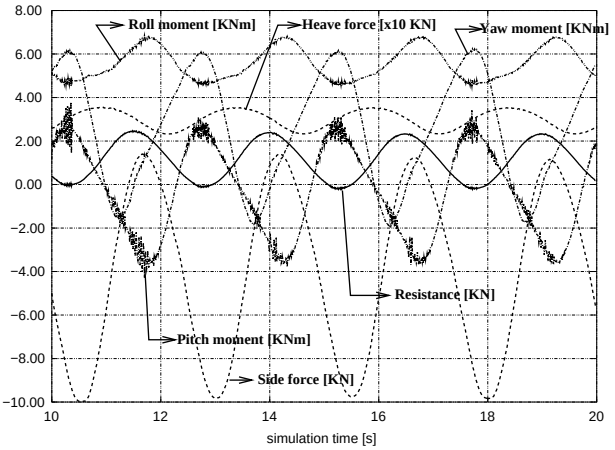

Figure 10. Forces and moments on boat sailing upwind in waves

The CPU time needed for computing the 20 s simulation time is 2.5 hours on a linux-cluster with 4 AMD 2000+ processors, or something less than 4 times that on a single processor. In this case the numerical grid for the whole boat with starboard and port side with about $200{,}000$ control volumes has to be used.

4.2 Boat reaching in quartering waves

For this simulation the same sailing attitude as in the preceeding example was set ($\varphi = -15°$, $\beta = 4°$ and $v_o = 3.5$ m/s). The heeling moment and driving force were kept unchanged as well. The wave parameters were the same as before but $\mu = 45°$ (waves from the Bb quarter). The resulting frequency of encounter is $\omega_e = 0.98$ s^{-1} ($T_e = 6.4$ s) so that more seconds simulation time are needed to obtain enough wave encounters.

Figure 11 shows the motions for this reaching condition in waves. Up to 20 s 3 DOF were free – heave, pitch and roll – while the surge was released thereafter (surge and v_{sea} curves constant up to 20 s). As expected for following waves, the mean boat speed increases and the boat surges forward. The pitch angle oscillates between about $-3°$ and $+3°$, i.e. more symmetric than in the head waves case. The roll angle oscillates between about $-3°$ and $-20°$, that means much more than in the head waves case. The resulting motions are in general not sinusoidal, since the non-linear, coupled equations of motions are solved here without any linearization. The roll motion curve for instance shows small non-linearities and coupling with other motions. The heave oscillates between about -0.2 m and $+0.2$ m. This suggests greater numerical dissipation of the wave amplitude than in the head waves case, in part because the flow-boundary in the wake is further away than the front boundary, but more importantly, because the waves are more difficult to generate backwards from the outlet or wake boundary than from the front boundary. This point needs to be clarified and

the generation of following waves still has to be improved.

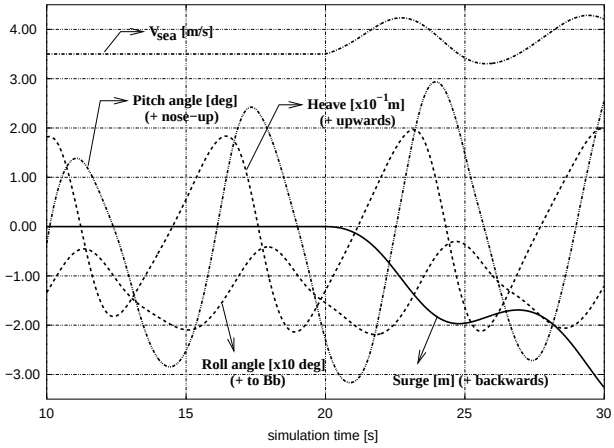

Figure 11. Motions of boat reaching in quartering waves

Figure 12 shows the corresponding forces and moments for the 6 DOF. In this case (quartering waves), the yaw moment is still larger than for the head waves case. Note that the roll moment and side force show some complicated coupling with the other motions as well.

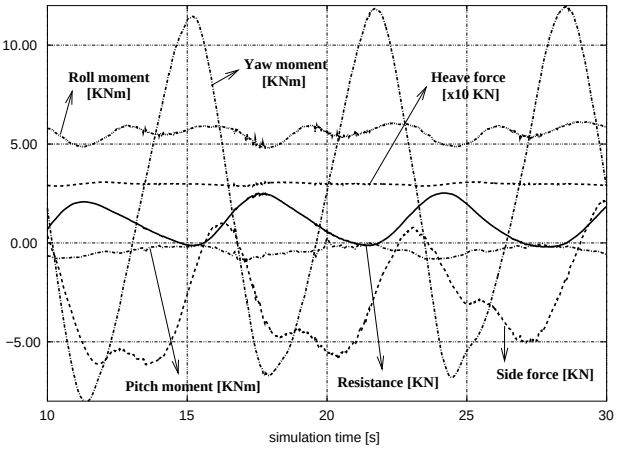

Figure 12. Forces and moments on boat reaching in quartering waves

Figure 13 shows one instant of the simulation by $t = 23.5$ s, where the different gray shades indicate the water elevation. The best impression of the motions can be obtained by analysing the video animations (mpeg-files can be downloaded from www.azcueta.net).

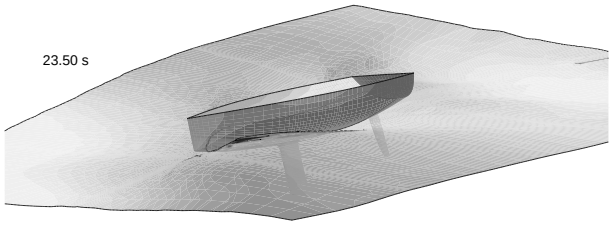

Figure 13. Boat reaching in quartering waves

4.3 Boat reaching in beam waves

The last example presented here is for the boat in the same sailing attitude and with the same wave parameters as the previous one but in waves coming from the port beam ($\mu = 90°$). The frequency of encounter in this case is the same as the wave frequency $\omega_e = 1.75$ s^{-1} ($T_e = 3.6$ s). 3 DOF were set free: Heave, roll and pitch. Figure 14 shows the motions over 20 s simulation time. The initial phase of the simulation is also shown. Over the first two periods the motions are still not periodical, since the waves have to build up first. In the diagram one can observe that especially the pitch angle is coupled with the other motions.

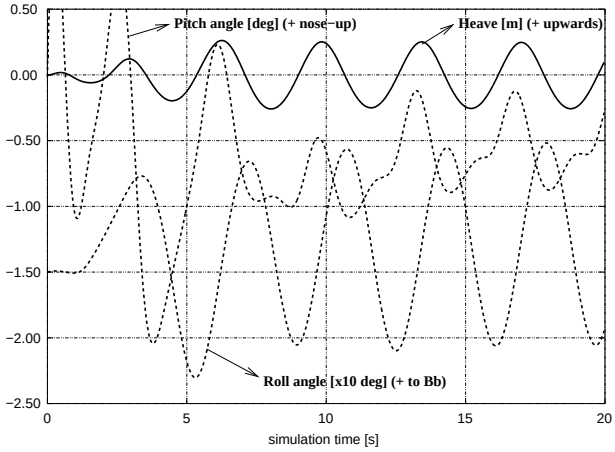

Figure 14. Motions of boat reaching in beam waves

Figure 15 shows the wave contours around the boat at one time instant of the simulation ($t = 15.4$ s). One can see that the incident waves are coupled with the wave pattern of the boat. The incident waves are not parallel to the side boundary, since μ is measured relative to the course and the mesh is rotated by the leeway angle $\beta = 4°$.

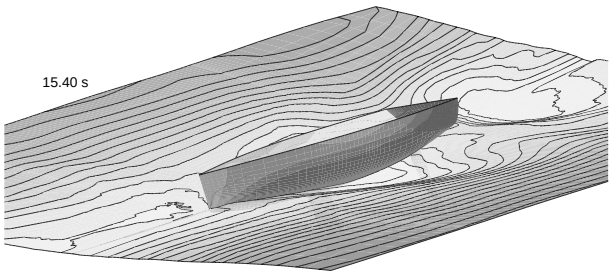

Figure 15. Boat reaching in beam waves

Several other configurations of sailing attitude and wave parameters were simulated, such as for the boat upright or with leeway and roll angle in following waves ($\mu = 0°$), but since no new conclusions could be drawn so far they are not presented here.

5. CONCLUSIONS AND PLANNED WORK

The simulations presented here have not been applied so far for production runs to optimize hull shapes, but they are intended to show some of the possibilities which are about to arise through Navier-Stokes simulations for such purposes in the near future. Although the methods are not really mature yet, their potential is great and it is a matter of time until they find their way into the design offices.

Much effort need still be made to enhance the free-surface computations, since the free-surface deformation is usually responsible for scatter in the results – due to wave oscillation and reflection at the boundaries – which makes a thorough analysis more difficult. Furthermore, validation with model or full-scale measurement still remains imperative.

To achieve high accuracy in performance prediction is not the only objective of these sort of computations, but also to be able to rank concurrent designs correctly, and it is in this area that the numerical methods prove to be more efficient. One example of a useful application for the kind of resistance tests presented here, whose sensitivity makes them capture small differences in resistance, could be to systematically investigate the effects of shifting the longitudinal centre of mass of the boat for different heel angles to find its optimum positions. This information can then be made available on board to support the sailor's intuition to trim the boat to sail fast. Another example is of course systematic variations of hull shape to optimize the design. It is especially for the optimization of appendages neglecting the free-surface that this approach could be applied most efficiently, since the above mentioned problem of scattered results does not apply here. For appendage optimization it is imperative though to improve the turbulence modelling to account to some extent for the laminar effects and transition. This will also be an area of further investigations.

In the present simulation the air flow acting on the topsides is solved as well. The flow velocity in the air was set equal to the water velocity or boat speed, i.e. a no-wind condition applied. With the VOF method employed here, however, there is no restriction to set a realistic wind gradient above the water through appropriate boundary conditions. The final goal would then be to simultaneously compute the water flow and the air flow around the sails, until the balance of forces is achieved. RANSE computations for sail design is obviously an area of intensive research at the moment. While this is an ambitious goal for the future, a simpler aerodynamic module like those used by VPPs will soon be implemented to supply the instantaneous sail forces instead of setting them constant like in the present simulations. Course stability could be achieved by implementing a course controller algorithm to provide the steering moments or to control the angle of a movable rudder embedded into a rotating grid block with sliding interface.

The planned work on wave induced motions is to improve the generation of quartering and following waves, to simulate boat responses in 6 DOF including sway and yaw, and to extend the method to simulate the boat motions in irregular seaways generated according to a given directional spectrum. In order for these simulations in irregular seas to be useful, a statistical analysis of the motions is needed. To make this possible a simulation time of the order of one hour (instead of the 20 to 30 seconds of the present simulations) would be necessary. With the computer power used for this work this would take around 18 days CPU for each mean wave direction and boat speed. Although this figure is not really encouraging for practical purposes, with some simplifications and growing computer power it may be worthwhile the effort in the future.

References

[1] Azcueta, R. (2001), *"Computation of Turbulent Free-Surface Flows Around Ships and Floating Bodies"*, PhD. thesis, Technical University Hamburg-Harburg.

[2] Azcueta, R., Muzaferija, S. & Perić, M. (1999), "Computation of Breaking Bow Waves For A Very Fat Hull Ship", *7th International Conference on Numerical Ship Hydrodynamics*, Nantes.

[3] Ferziger, J. H. & Perić, M. (1996), *Computational Methods for Fluid Dynamics*, Springer, Berlin.

[4] Brandt, H., Hochkirch, K., Abdel-Maksoud, M. & Frölich, M. (1997), "Leistungsanalysen für das Segeldynamometer", *Jahrbuch der Schiffbautechnischen Gesellschaft (STG)*, Vol. 91, Hamburg.